

Self-assembly of chiral diketopyrrolopyrrole chromophores giving supramolecular chains in monolayers and twisted microtapes

Joshua Humphreys^{1,2}  | C. Elizabeth Killalea^{1,2}  | Flavia Pop^{1,2}  |
E. Stephen Davies² | Giuliano Siligardi³  | David B. Amabilino^{1,2,4} 

¹The GSK Carbon Neutral Laboratories for Sustainable Chemistry, The University of Nottingham Jubilee Campus, Nottingham, UK

²School of Chemistry, University of Nottingham, Nottingham, UK

³Diamond Light Source, Harwell Science and Innovation Campus, Didcot, Oxfordshire, UK

⁴Institut de Ciència de Materials de Barcelona (ICMAB-CSIC), Campus Universitari de Cerdanyola, Barcelona, Spain

Correspondence

David B. Amabilino, Institut de Ciència de Materials de Barcelona (ICMAB-CSIC), Campus Universitari de Cerdanyola, Barcelona 08193, Spain.
Email: amabilino@icmab.es

Present address

Flavia Pop, MOLTECH-Anjou, UMR 6200, CNRS, University of Angers, Angers, France.

Funding information

Engineering and Physical Sciences Research Council, Grant/Award Number: EP/M005178/1; University of Nottingham, Grant/Award Number: BNSCF421

Abstract

Chiral diketopyrrolopyrroles appended with enantiomeric ethyl lactate functions through an ether linkage to the aryl backbone of the chromophore were synthesized via the Mitsunobu reaction. The molecules have good solubility and excellent optical properties, high molar absorption coefficients, and fluorescence quantum yields. Helical aggregates with circular dichroism arising from the supramolecular arrangement are seen in both solution and thin films, and the aggregates also display circularly polarized luminescence ($g_{lum} \approx \pm 0.1$). The molecules assemble to give monolayers on graphite and precipitate from solution forming supramolecular twisted tapes hundreds of microns long.

KEYWORDS

aggregation, hydrogen bonds, morphology, scanning tunnelling microscopy

1 | INTRODUCTION

A supramolecular approach to the design of organic electronic materials has been proposed and investigated

for well over two decades as a strategy to produce highly efficient optoelectronic devices.^{1–8} At the basic level, there are two key areas that this approach looks to improve upon regarding existing technology: active

[This article is part of the Special issue: Chiral Materials. See the first articles for this special issue previously published in Volumes 34:12, 35:2, 35:3 and 35:4. More special articles will be found in this issue as well as in those to come.]

This is an open access article under the terms of the [Creative Commons Attribution](https://creativecommons.org/licenses/by/4.0/) License, which permits use, distribution and reproduction in any medium, provided the original work is properly cited.

© 2023 The Authors. *Chirality* published by Wiley Periodicals LLC.

layer morphology and charge carrier transport. In organic solar cells, morphological control ideally sees the checkerboard pattern employed,^{9,10} which would see large contact between donor and acceptor domains allowing exciton splitting into free charge carriers and efficient charge transport to electrodes. Non-covalent interactions, namely, π stacking¹¹ and hydrogen bonding,^{4,12} have been shown to influence charge mobility in organic materials, and incorporation of these motifs onto chromophores, coupled with the introduction of chirality, has seen the manifestation of a number of superstructure architectures from liquid crystals¹³ to gelators,¹⁴ ribbons,¹⁵ nanocrystals,¹⁶ and nanowires.¹⁷ Hence, the design of supramolecular electronic materials looks to exploit this ordering to create reproducible, idealistic active layer morphologies between donor and acceptor domains as a means to improve charge transport and efficiency in next-generation optoelectronic devices.^{18,19}

In the context of organic semiconductors, over recent years, diketopyrrolopyrrole (DPP) has come to the fore as a well-explored material, with simple synthetic transformations resulting in substantial modulation of properties.^{20,21} This has led to the development of highly efficient organic electronic devices ranging from solar cells to transistors to organic light emitting diodes (OLEDs).^{22–26} Broadly speaking, the aryl substituent, in the most part, typically dictates the intended application of the DPP molecule, with thiophene-based systems (**ThDPP**, Supporting information S1: ESI 5.1) being used for organic electronic applications thanks to their planarity, good charge transport, and straightforward polymerization, whereas phenyl-based systems (**PhDPP**, Supporting information S1: ESI 5.1) are synonymous with sensors and imaging agents given their excellent emissive properties in both the solution and the solid state.^{27–37}

For DPP systems, there have been several strategies to impart hydrogen bonding³⁸ and chiral motifs^{39–41} that promote self-assembly and modulate π - π stacking interactions, to ultimately evaluate their impact on the compounds' optoelectronic performance. DPPs inherently suffer from solubility issues given the strong intermolecular interactions driven by π - π stacking and hydrogen bonding through the lactam moiety. Hence, to study hydrogen bonding in solution-processable organic electronic devices, much of the early work in this area looked to use thermocleavable groups attached at the lactam nitrogen that would increase solubility to allow thin film deposition from solution followed by thermal annealing to release the hydrogen-bonding network.^{42–46} Mono-alkylation of the DPP unit has been explored also, with these more soluble derivatives

displaying cofacial π stacks that show improved mobility versus the herringbone structure often adopted by the dialkylated form.^{47,48} Additionally, the introduction of alkyl chains containing hydrogen-bonding amide and urea groups at the lactam nitrogen has been reported.^{46,49–54} Alternative functionalization along the aryl backbone through the Knoevenagel condensation reaction with amide and semicarbazone motifs has been described for **ThDPP**-based systems.^{55–58} With regard to chirality, alkyl, amide, and amino acid side chains have been typically introduced through *N*-alkylation at the lactam.^{59–64} Additionally, end capping of the aryl system to give axially chiral systems with promising circularly polarized luminescence (CPL) properties has been detailed.^{65–68} Imparting said motifs that promote self-assembly on to the DPP skeleton has seen systems that form gels,^{62,69,70} nanowires,⁷¹ and liquid crystals^{72,73} among others.

Despite the generalization that **PhDPP** systems are less suited as standalone optoelectronic materials relative to **ThDPP**, Glowacki *et al.* previously investigated **PhDPP NH** semiconductors and suggested promising mobility values.³⁴ Little has been explored since, possibly because of the molecule's poor solubility. For **PhDPP**, *N*-alkylation leads to soluble, highly emissive materials, at the expense of forming twisted molecular backbones (attributed to the steric clash between the phenyl-appended protons and the *N*-substituents) that have reduced mobility, absorption, and large band gaps relative to their parent chromophore.⁷⁴ They are generally regarded as being less favorable as standalone materials in devices but potentially interesting as morphological additives.^{70,75} From a theoretical perspective, it has been suggested that, based on calculated mobilities from **PhDPP**-based crystal structures, these systems hold promise to rival rubrene as organic field effect transistor (OFET) materials, with the challenge of optimization of device engineering the main obstacle.⁷⁵ In light of this hypothesis, and taking into account that retention of the free lactam and functionalizing along the backbone with phenyl ethers has seen derivatives with improved solubility that self-assemble to form lamellar homo assemblies dominated by hydrogen bonding between lactams,^{72,73,76,77} we proposed potentially functionalizing the DPP backbone with chiral esters to impart solubility and investigate the influence of chirality and hydrogen bonding of the lactam core on the supramolecular assembly of the system as a means to potentially address the challenge of active layer morphological control and charge transport in organic electronics. Thus, herein, we describe the synthesis of a novel DPP system appended with enantiomeric non-racemic ethyl lactate functions through an

ether linkage and characterize the optoelectronic properties and self-assembly in the solution, at an interface, and in the solid-state, to aid in development of future supramolecular organic electronic materials.

2 | RESULTS AND DISCUSSION

2.1 | Synthetic procedure

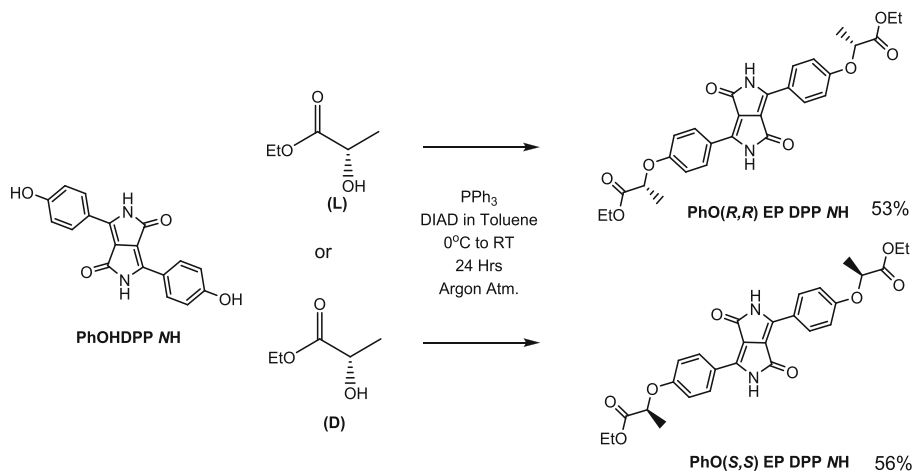
The core phenol-appended DPP compound (**PhOHDPP NH**) was synthesized according to previously published methods.^{73,78} Once isolated, we wished to functionalize the phenol moiety with chiral substituents to introduce asymmetry, increase solubility, and maintain the ability of the core to enter into hydrogen bonding. The chain used here is ethyl lactate, which is commercially available as both enantiomers and can be post-functionalized to create other chiral hydrogen-bonding materials such as acids (Supporting information S1: ESI 5.2) and amides. The (–)-ethyl L-lactate (*S* enantiomer) was explored first, because as the natural isomer it is cheaper. The proposed route to achieve the ether formation was via the Mitsunobu reaction,^{79,80} to ensure stereoselectivity and avoid basic reagents that might react with the lactam NH, which leads to undesired products.⁷³ We, among many, have already shown that this reaction is highly stereoselective with enantiomeric excesses typically over 90 for this kind of phenol-lactate coupling.^{81–83} To optimize the reaction, fresh bottles of ethyl lactate and coupling agent were used, and the solvent dried exhaustively, and purification by Soxhlet extraction followed by precipitation was required to maximize the purity in one case. We were unable to identify the impurity after only precipitation (although it does affect the optical activity, see below). After optimization, the reaction (Scheme 1) proceeded well to produce the novel chiral system **PhO(R,R) EP DPP NH** in good yield (53%), with inversion of

stereochemistry. The solubility of the compound at room temperature is good in solvents such as dimethylsulphoxide (DMSO), *N,N'*-dimethylformamide (DMF), diglyme, and tetrahydrofuran (THF). The opposite enantiomer (**PhO[S,S] EP DPP NH**) was also synthesized, using (+)-ethyl-D-lactate (*R* enantiomer), under identical conditions (Scheme 1). The compounds showed better solubility compared with the parent compound **PhOHDPP NH**. Although we were unable to check the enantiomeric excess of the chiral compounds made here (their high polarity and their limited solubility in appropriate solvents for chromatography made this impractical in our hands), the optical activity observed by circular dichroism (CD) spectroscopy indicates similar enantiopurity (see below). Despite appearing clean by nuclear magnetic resonance spectroscopy (NMR) and elemental analysis, the first attempts at synthesis of **PhO(R,R) EP DPP NH** and **PhO(S,S) EP DPP NH** resulted in compounds that exhibited slightly different CD spectra (and only **PhO(S,S) EP DPP NH** gave rise to a CPL signal in the first isolated materials, see below), indicating a slight chemical or optical impurity.^{84,85} The fact that after optimization the compounds were purified by precipitation, a process that would be expected to favor a high enantiomeric purity, and the process does give materials with mirror image CD spectra, supports that hypothesis. The subsequent characterization proved the identity and chemical purity of the compounds (see Supporting information S1: ESI for details).

2.2 | Optical properties

2.2.1 | Solution-state absorption properties

In solution, both **PhOHDPP NH** and **PhO(R,R) EP DPP NH** possess a two band absorbance profile typical of donor–acceptor systems of this type (Figure 1).⁸⁶ The



SCHEME 1 Reaction conditions used for the synthesis of **PhO(R,R) EP DPP NH** and **PhO(S,S) EP DPP NH**.

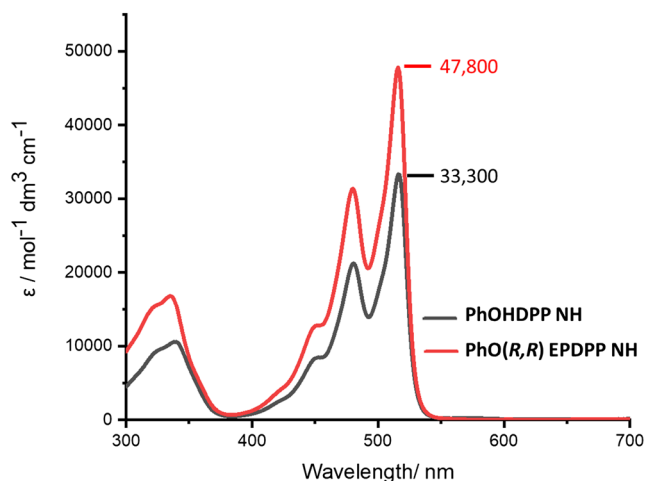


FIGURE 1 UV-visible absorption spectra of **PhOHDPDPP NH** and **PhO(R,R) EPDPP NH** in DMSO (2.2×10^{-5} Mol dm $^{-3}$).

vibronic structure to the absorption band indicates the relative planarity, with little variation between the systems, indicating similar frontier orbital energies and band gaps.^{87–91} Functionalization with the ethyl propionate motifs leads to a near 50% improvement in ϵ in DMSO (Figure 1) compared to the phenol precursor, with the highest observed value of $54,100 \text{ dm}^3 \text{ mol}^{-1} \text{ cm}^{-1}$ in THF (Supporting information S1: ESI 5.4), showing marked improvement versus **PhDPP NH** and similar unfunctionalized lactam DPP derivatives.^{91,92} This property suggests good viability for light-harvesting applications, giving comparative absorptivity to known highest absorbing **ThDPP** materials in the literature,^{33,93} which have been successfully incorporated into optoelectronic devices.⁹⁴

2.2.2 | Solution-state emissive properties

As with absorption, **PhO(R,R) EPDPP NH** displays characteristic emissive behavior exhibited by other **PhDPP NH** analogs,^{74,90,91,95} with mirror image absorption and emission profiles and retention of vibronic structure (Figure 2). This feature is indicative of a highly planar molecule in both the ground and the excited state, with a small difference in energy between the 0–0 vibronic transitions in absorption and emission, manifesting in a small Stokes shift (6 nm). The compound is highly emissive, indicated by the quantum yield (Supporting information S1: ESI 5.4), showing one of the highest values recorded for unfunctionalized lactam DPPs (89%).^{33,96,97} The emission is quenched in the solid state, presumably because of the proximity of the aromatic cores in this phase.⁷⁴

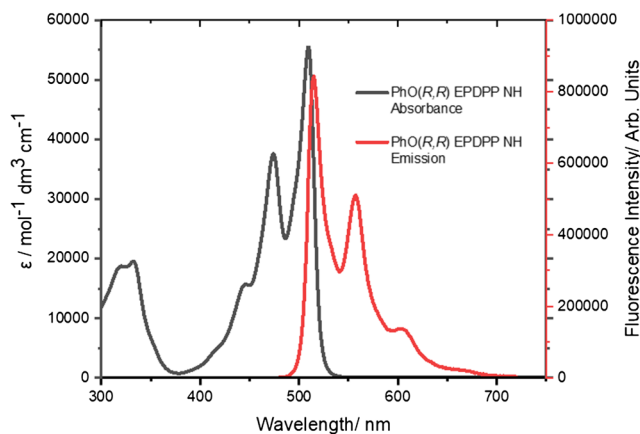


FIGURE 2 UV-visible absorption and emission spectra of **PhO(R,R) EPDPP NH** in THF. Excitation wavelength 470 nm.

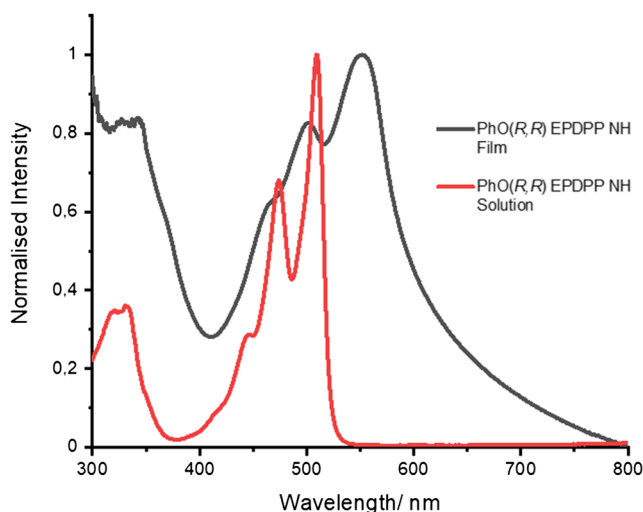


FIGURE 3 UV/Vis absorption spectra of **PhO(R,R) EPDPP NH** in solution in THF and a drop-cast thin film from THF.

2.2.3 | Solid-state absorption properties

Solid-state absorption spectroscopy is a useful tool to determine the arrangement of DPPs of this type in thin films.⁷⁴ To prepare the samples, concentrated solutions of the compounds in THF (0.5 mg/ml) were drop-cast onto glass, and the solid-state absorption spectra were recorded. In both cases (Figure 3 and Supporting information S1: ESI 5.5), there is a bathochromic shift (42 nm) and a visible broadening of the film spectrum relative to the solution. These effects are attributed to close intermolecular interactions in the solid state, aided by hydrogen bonding that is observed by infrared (IR) spectroscopy (see below).^{34,98} The bathochromic shift in the film indicates that the molecules stack in a head-to-tail orientation, suggesting *J*-type

aggregation. From the absorption edge of the film (602 nm), the band gap is calculated to be ~ 2.0 eV (Supporting information S1: ESI 5.6).

2.3 | Redox properties

To assess donor–acceptor capability, frontier orbital energies were estimated from cyclic voltammetry measurements. The voltammograms demonstrate that **PhO(R,R) EP DPP NH** has an irreversible oxidation, shown by the absence of a return wave (Supporting information S1: ESI 5.7). Indeed, the voltammograms performed with different scan rates (Supporting information S1: ESI 5.8 and 5.9) suggest that the species generated either by oxidation or by reduction have poor stability under the conditions of the experiment. The oxidation appears to be a two-electron process from the current magnitude, and we suggest that the dication system will form a quinoidal-type structure similar to those observed for other DPP systems.^{99–102} The two-electron process indicates the system's electron richness and potential as an electron donor system. Previously, we observed that for the two-electron oxidation of **PhOMeDPP N-Hex** and **PhOHDPP N-Hex**, the presence of an acidic hydrogen atom in the latter destabilizes the radical cation,⁷⁴ which could also be the case here from the lactam hydrogen atom. The electron-accepting ability is indicated by the single one-electron quasi-reversible reduction process (Supporting information S1: ESI 5.7–5.9).

Both **PhO(R,R) EP DPP NH** and its enantiomer (that displays identical voltammetric behavior) possess highest occupied molecular orbital (HOMO) and lowest unoccupied molecular orbital (LUMO) energy level values typical of a donor system, with an electrochemical band gap of 1.96 eV,⁹ giving good agreement with the optical band gap (Table 1) and a comparable band gap to other lactam-free DPPs, namely, **PhDPP NH**, **PhCIDPP NH**, and **PhBrDPP NH** (2.1 eV) (Supporting information S1: ESI 5.11), which all displayed good mobility values.³⁴

2.4 | Formation of twisted microtapes

Whereas solubility of the compounds is excellent in certain solvents, controlled cooling and vapor diffusion techniques in solvents of medium polarity lead to intriguing aggregated species. Whereas it is largely insoluble at room temperature in acetone, acetonitrile, and methanol, warming leads to complete dissolution of the compounds to give yellow solutions, from red powders (Figure 4). Cooling leads to the formation of red flocculant-type solids that were analyzed using different microscopes. The formation of the aggregates, kinetically determined in a similar way to crystal growth, is characteristic of other micron-scale objects.¹⁰³

Visualization of the solids formed by the individual enantiomers by polarizing optical microscopy showed that they comprised fibers with helical nature (Figure 5). Transmission micrographs show relatively featureless red fibers that are either straight (for the thicker objects) or curved, and all of them are dozens of microns in length, at least. Crossed polarizers inserted into the transmitted

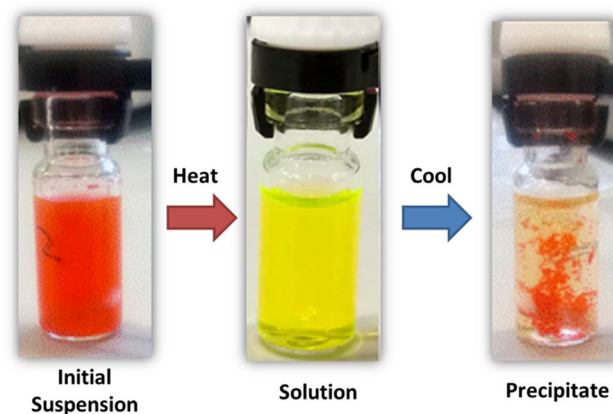


FIGURE 4 Photographs showing the appearance of an initial suspension of **PhO(S,S) EP DPP NH** after sonication at room temperature, the solution of the compound near the boiling point of the solvent, and the flocculant appearance of the suspension containing a precipitate of helical aggregates after slow cooling.

TABLE 1 Experimental frontier orbital energy levels determined through cyclic voltammetry measurements in solution and optical band gap from thin film absorption edge for **PhO(R,R) EP DPP NH**.

Compound	Oxidation onset [V]	Reduction onset [V]	HOMO [eV]	LUMO [eV]	Electronic E_g [eV]	Optical E_g (film) [eV]	LUMO (film) [eV]
PhO(R,R) EP DPP NH	0.300 ^a	−1.66 ^a	−5.10 ^a	−3.14 ^a	1.96 ^a	2.06 ^b	−3.04 ^b

^aDetermined from cyclic voltammetry measurements in solution of compound (1 mmol), electrolyte (tetrabutylammonium hexafluorophosphate, 0.1 M) in DMF. Values referenced against the ferrocenium–ferrocene redox couple.

^bThin films were formed on glass slides by drop casting of a concentrated THF solution (0.5 mg/ml).

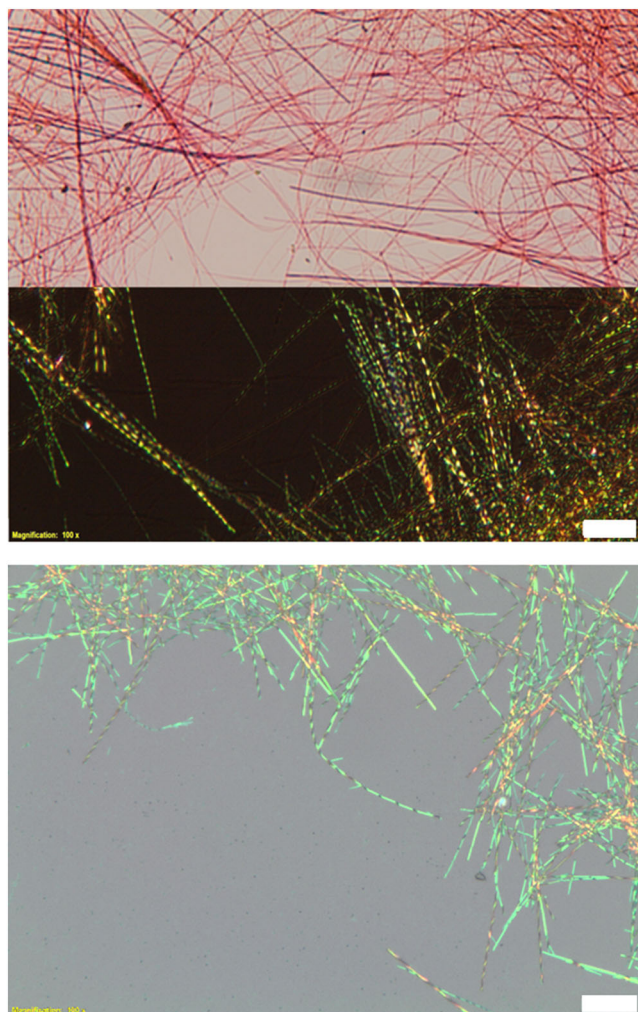


FIGURE 5 Optical microscope images (scale bars correspond to 5 μm) in transmission (top showing unpolarized and cross-polarized images, the latter with the typical banded feature of helical objects) and reflectance mode of **PhO(*R,R*) EP DPP NH**, grown from acetonitrile (top) and acetone (below) solutions under variable temperature conditions showing the general morphology and twisting of the fibers.

light beam show that the objects change regularly and periodically, giving banded features, indicative of regular twisting. The reflected light optical micrographs show the helical features most clearly.

Optimization of conditions to form these fibers was undertaken through solvent screening studies. We determined that ≈ 0.5 mg/ml solutions of either enantiomer in acetone, methanol, ethanol, or acetonitrile all lead to the formation of helical aggregates over time, after initial sonication to disperse in the media, followed by heating to solubilization and slow cooling. Minimum aggregation concentrations and optimal cooling rate were determined using a Crystal16 parallel crystallizer, which allowed

greater precision to control heating and cooling rate, coupled with qualitative analysis through optical microscopy. Through these means, an optimal cooling rate of $1^\circ\text{C}/\text{min}$ or slower after complete solubilization was seen to be crucial for the formation of well-defined twisted structures.

Faster cooling led to much smaller aggregates, for which helicity could not be determined by optical methods. This observation suggests that the fibers are formed under kinetic control rather than thermodynamic.¹⁰⁴ The minimum concentration for the formation of well-defined helical structures was seen to be in the range 0.1–0.2 mg/ml, depending on solvent system (Supporting information S1: ESI 5.12). Initial growth was determined through a change in turbidity upon cooling of the solution, typically seen to be $5\text{--}10^\circ\text{C}$ below the boiling point of the solvent (Supporting information S1: ESI 5.13). Additionally, vapor diffusion of *tert*-butyl methyl ether into a 0.2 mg/ml THF solution of **PhO(*R,R*) EP DPP NH** or **PhO(*S,S*) EP DPP NH** also led to the formation of helical aggregates after several days (Supporting information S1: ESI 5.14), which could also be promising for post-deposition solvent annealing.^{105,106}

Optical microscope images (Figure 5 and Supporting information S1: ESI 5.15–5.23) detail the well-defined structures formed from variable temperature and vapor diffusion as mentioned previously. In reflectance mode (Supporting information S1: ESI 5.16–17), the opposite twist for each enantiomer is clearly seen, showing that molecular chirality is dictating the direction of the twist. From several images (Supporting information S1: ESI 5.24), it was seen that there are also quite a few fractured fibers resembling straight plates, a possible result of unwinding upon deposition on the surface. The helical fibers display birefringence at the node, but upon unraveling, the species no longer polarize the light, suggesting the materials have lost order. Seemingly thicker fibers form through bundling of smaller fibers together (Supporting information S1: ESI 5.22).

Twisted crystals of this nature have been observed in the formation of solids from a range of organic compounds, generally from the melt, and are surprisingly common.^{107–109} It is believed that over a quarter of simple molecular crystals can be grown with a twisted morphology from the melt,^{110–112} but those precipitated from solution are far rarer. Indeed, there are few examples where, like here, mesoscale twisting can be directly linked to the chirality of the crystallizing molecules.^{113,114} More usually, the connection between molecular chirality and supramolecular chirality is enigmatic, and there is no direct correlation between molecular and supramolecular chirality.¹¹⁵ There are currently several accepted mechanisms for the formation of twisted crystals, all of

which are united by the common theme of stress-relief.^{108,109} This stress can come from a variety of sources including dislocations as in the Eshelby mechanism; unbalanced surface stresses typically seen in polymers crystallized from the melt or heterometry stresses in the auto deformation mechanism.

Studies into the formation aggregates were also conducted with 50:50 mixtures of the two enantiomers through variable temperature and vapor diffusion, but no helicity was observed, and only straight, short plates were formed (Supporting information S1: ESI 5.25). This result indicates that the racemic compound is formed preferentially. It also indicates that the enantiomers have a high degree of optical purity, as the twisted objects seen by microscopy are very morphologically pure, enantiomeric

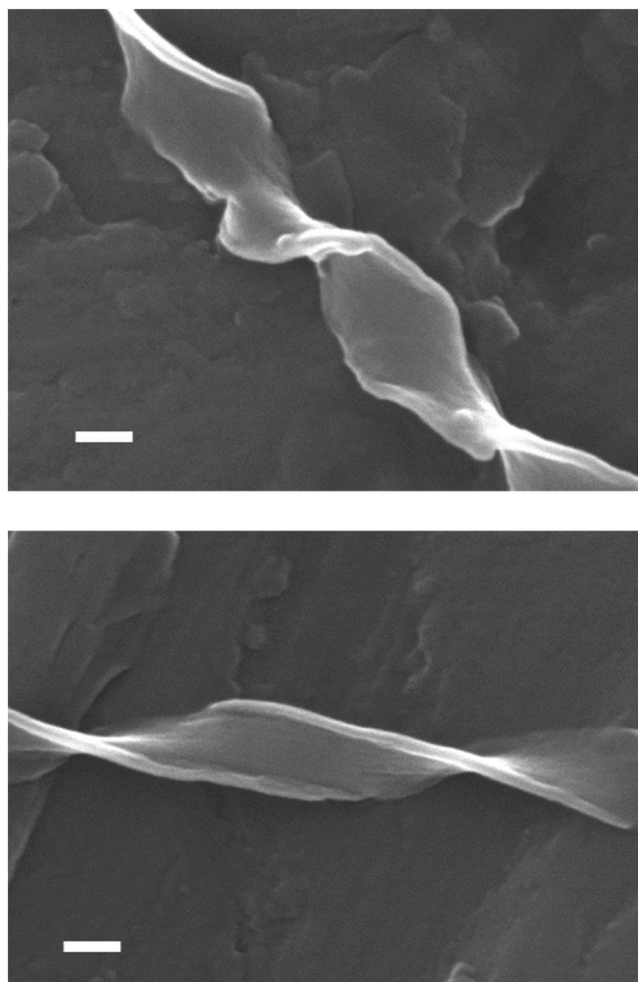


FIGURE 6 Scanning electron microscopy (SEM) image of **PhO(S,S) EP DPP NH** (top) and **PhO(R,R) EP DPP NH** (bottom), grown from acetone solutions under variable temperature conditions showing the general morphology and twisting of the fibers that are opposite for the two enantiomers. The scale bar corresponds to 100 nm.

impurities would be expected to lead to microscopic heterogeneity in the aggregates. Attempts to grow single crystals of **PhO(R,R) EP DPP NH**, **PhO(S,S) EP DPP NH**, or their mixture, through various techniques failed to produce any objects of sufficient size and quality for single crystal diffraction studies.

Given the promising optical microscope images, the chiral aggregates were further characterized using scanning electron microscopy (SEM). Figure 6 and Supporting information S1: ESI 5.26–5.45 show examples of micron-scale twisted tapes grown from acetone, acetonitrile, methanol, and vapor diffusion of *tert*-butyl methyl ether into THF for **PhO(R,R) EP DPP NH** and **PhO(S,S) EP DPP NH**, showing the previously mentioned opposing twists, dictated by point chirality of the molecule. The aforementioned bundling of fibers to make larger structures is seen most prominently in the acetonitrile grown fibers (Figure 7). As observed with optical microscopy in some cases, deposition onto the SEM stub leads to unraveling of fibers (Supporting information S1: ESI 5.45), and the relative thinness can be seen by the fact fibers, which are visible underneath.

There is generally a well-defined relationship between the pitch of the observed twisting and the dimensions of the crystalline objects as it has been shown that twisted crystals unwind as they grow.¹¹¹ Most systems exhibit a correlation of the pitch (P), and h is the smallest cross-sectional size, for example, the thickness of a ribbon^{108,109} with the exception of those grown via the Eshelby twist, which can be fitted to the function $P \sim h^2$.¹¹⁶ A twist-pitch analysis of fibers was therefore performed for both **PhO(R,R) EP DPP NH** and **PhO(S,S) EP DPP NH**

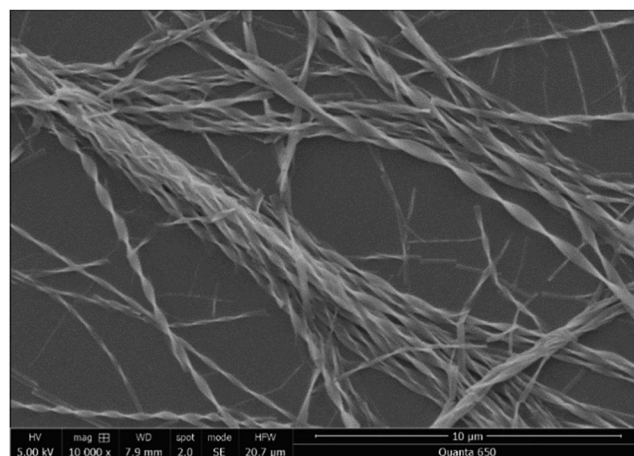


FIGURE 7 Scanning electron microscopy (SEM) image of **PhO(R,R) EP DPP NH** grown from an acetonitrile solution under variable temperature conditions showing the general morphology and twisting of the fibers.

structures formed from an acetone solution, and data can be fitted to the equation $P = kh^n$, where n is equal to 0.47 and 0.49, respectively, ruling out the Eshelby twist as their growth mechanism (Supporting information S1: ESI 5.46–5.48). Both data sets lie below the line $2P = 103\pi h$, and therefore, auto deformation and surface stresses can be at least partially relieved through twisting.

IR measurements of the evaporated films of the chiral DPP derivatives from the solution in THF, suspended aggregates in acetone, acetonitrile, and THF vapor diffused with *tert*-butyl methyl ether, showed identical spectra for the NH region, displaying only a signal corresponding to a hydrogen-bonded NH group,^{44,59,72,117} and no free amide NH, with similar findings for the carbonyl (Supporting information S1: ESI 5.49–5.50), showing that hydrogen bonding is driving aggregation.

2.5 | CD spectroscopy

CD measurements were undertaken in solution to deduce the optical activity of the enantiomeric DPP derivatives. Even at very high concentrations in THF, only weak optical activity is observed (see Supporting information S1: ESI 5.51–5.52), with no apparent concentration dependence, indicating that the CD signal arises as a result of the totally solvated monomeric species. Two main peaks are observed, one at low wavelength, 262 nm, and one at higher wavelength, 546 nm. There is little coupling between the stereogenic center and the main chromophores in the molecules in this kind of unit, where the peak at around 260 nm is also observed, corresponding to the phenyl-O-lactate unit.^{118,119}

Initial screening of media showed that substantial optical activity is observed in the solvent systems previously described to form chiral fibers, namely, acetone, acetonitrile, and ethanol. Solutions containing aggregates were prepared through heating to solubilization and slow cooling at $\approx 1^\circ\text{C}/\text{min}$. CD spectra in acetone showed opposing signs for each enantiomer, with a positive Cotton effect at ≈ 565 nm ($\Delta\epsilon$ 3.4) for **PhO(R,R) EP DPP NH** and a second positive Cotton effect at 352 nm ($\Delta\epsilon$ 2.2). Upon heating, loss of optical activity and the *J*-aggregate band at ≈ 550 nm in absorption (Supporting information S1: ESI 5.53–5.57) ensues, owing to dissolution of the aggregate and return to the monomeric form. Relatively fast cooling ($2.5^\circ\text{C}/\text{min}$) fails to regenerate the signal of the aggregate confirming previous finding that a cooling rate of $1^\circ\text{C}/\text{min}$ or lower is required to form helical structures (Supporting information S1: ESI 5.55). Owing to the UV cut off of acetone and its volatility, ethanol was chosen for further study. The solution was first heated to 75°C , and the CD spectra were recorded, but

the compounds are not fully solubilized at this concentration, and so complicated multisignate spectra are observed (Supporting information S1: ESI 5.58–5.59). Both enantiomers exhibit a bisignate exciton couplet that has a center at 275 nm, which can be attributed to the coupling between the π - π^* transition dipole moments. **PhO(R,R) EP DPP NH** and **PhO(S,S) EP DPP NH** exhibit negative and positive exciton couplets, respectively, at this wavelength.

The restriction of flexibility that occurs upon aggregation of these molecules into chiral macrostructures could be the reason that complicated multisignate Cotton effects are observed at the low-energy end of the spectrum.¹²⁰ At this temperature, CD relative to the *J*-aggregate is minor compared with higher energy bands. The solution was cooled to 5°C at a rate of 1°C per min and aggregation ensued. As was the case in acetone, CD spectra at this temperature exhibit two large Cotton effects, which are an order of magnitude greater than seen at the lower temperature, with maxima at 355 and 567 nm, both of which are positive for **PhO(R,R) EP DPP NH** and negative for **PhO(S,S) EP DPP NH** (Figure 8), accompanied by a *J*-aggregate band at ≈ 550 nm observed in the absorption spectra⁵⁹ (Supporting information S1: ESI 5.60). There is little CD signal at the wavelength of the main absorption band in both solvent systems. A considerable increase in $\Delta\epsilon$ is observed for both signals in ethanol when compared with acetone ($\Delta\epsilon \approx \pm 15$, $\Delta\epsilon \approx \pm 7.5$ vs. $\Delta\epsilon \approx \pm 3.4$, $\Delta\epsilon \approx \pm 2.2$).

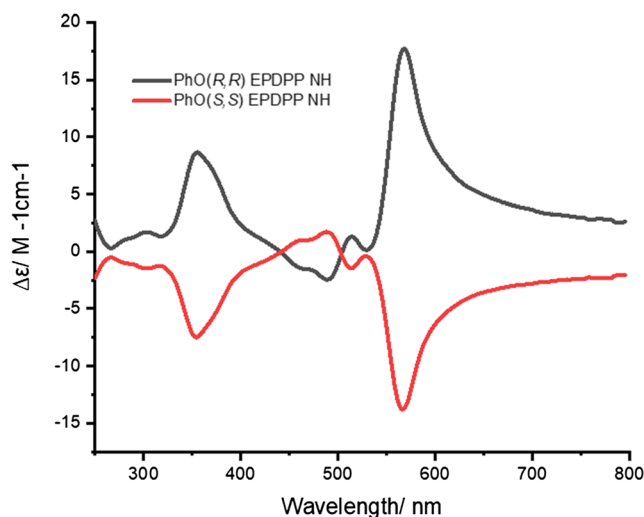


FIGURE 8 Circular dichroism spectra of **PhO(R,R) EP DPP NH** (black) and **PhO(S,S) EP DPP NH** (red) in 0.35 mmol solutions of ethanol at 5°C .

2.6 | Circularly polarized luminescence

The strong CD observed and the excellent emissive properties of the system prompted us to investigate the CPL of these derivatives in ethanol. Both enantiomers exhibit circularly polarized luminescence, with peaks at 550 nm corresponding to the 1–0 vibronic transition of the fluorescence spectra (Figure 9 and Supporting information S1: ESI 5.61) and equivalent to the wavelength of the *J*-aggregate in absorption. **PhO(S,S) EP DPP NH** displays a positive CPL signal, whereas **PhO(R,R) EP DPP NH** displays a negative one, opposite to CD. Literature studies of β - γ -enones attribute this unusual attribute to a reversal

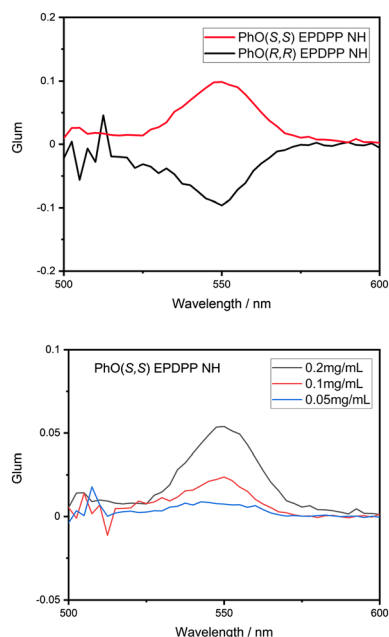
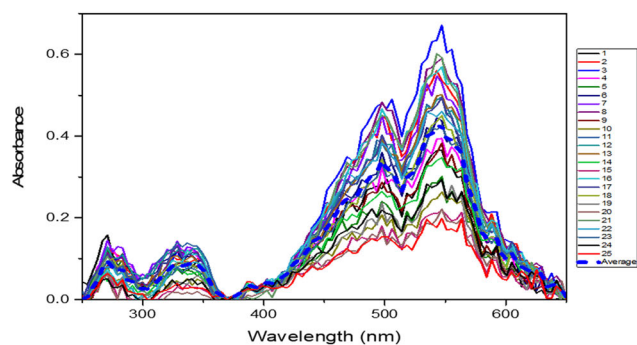


FIGURE 9 Circularly polarized luminescence (CPL) spectra of **PhO(R,R) EP DPP NH** (red) and **PhO(S,S) EP DPP NH** (black) in 0.35 mmol solutions in ethanol (top) and CPL spectra of **PhO(S,S) EP DPP NH** in acetone at different concentrations.



of local chirality between the ground and the excited state, for which additional interactions of the excited state are responsible.^{121,122} G_{lum} values of $\approx \pm 0.1$ show marked improvement compared to previously reported DPP systems.^{66,68} This high asymmetry in CPL is a result of aggregation, as the solution in THF shows no detectable CPL signal. In addition, recording the CPL for the (S,S) enantiomer in acetone at different concentrations revealed a dependence of the intensity on this factor (Figure 9). These data therefore support an aggregation-induced CPL mechanism, similar to that seen previously,^{123,124} and whose origin must lie in the asymmetry induced in the chromophores upon their self-assembly, in a conceptually similar manner to increased CD on aggregation.

2.7 | Solid-state CD

Given the promising chiroptical absorption properties in solution and the ambition to produce materials for organic electronics, thin films were deposited by drop casting a 2 mmol THF solution of **PhO(R,R) EP DPP NH** onto a quartz disk to study CD in the solid state (Supporting information S1: ESI 5.62). We considered that it would be interesting to use a mapping technique to study the apparent CD spectra over an area of the sample.^{125,126} Therefore, the CD spectra were recorded in imaging mode using the Module B spectrophotometer at B23 beamline for synchrotron Radiation CD (SRCS) of Diamond Light Source,¹²⁷ which can be used to map optical activity in solid films^{128,129} with a resolution of approximately 50 μ m. Therefore, the optical activity of any microscopic objects cannot be resolved, but the overall CD signal can be mapped in the regions of interest.

As seen (Figure 10), the film gives rise to two positive Cotton effects at 308 and 562 nm at room temperature, with the latter having a significantly greater intensity. The

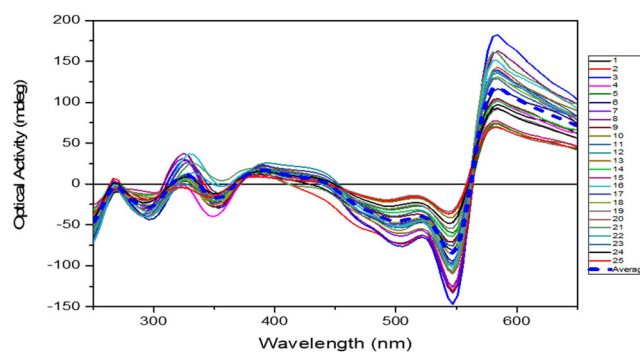


FIGURE 10 Circular dichroism spectra of 25 scans (step size of 50 μ m) and average (blue dotted line) of a drop cast film from a 2.00 mmol solution of **PhO(R,R) EP DPP NH** in THF.

Cotton effect at 562 nm coincides with the solid-state absorption maxima (Figure 3, Supporting information S1: ESI 5.63). Compared with the solution-state CD spectra, the main difference is in the 500–600 nm region where in solution there is a positive Cotton effect and in the solid state a positive excitonic couplet. The wavelength at which the strongest optical activities were observed was plotted

as 2D color maps to look at the distribution of the film (Figure 11), which show homogeneous distribution of the sign of the optical activity at any given wavelength, whereas the magnitude varies in a way that does not match exactly the absorbance of the films. These imaging CD experiments therefore show a heterogeneity in the supramolecular arrangement of the molecules in the film.

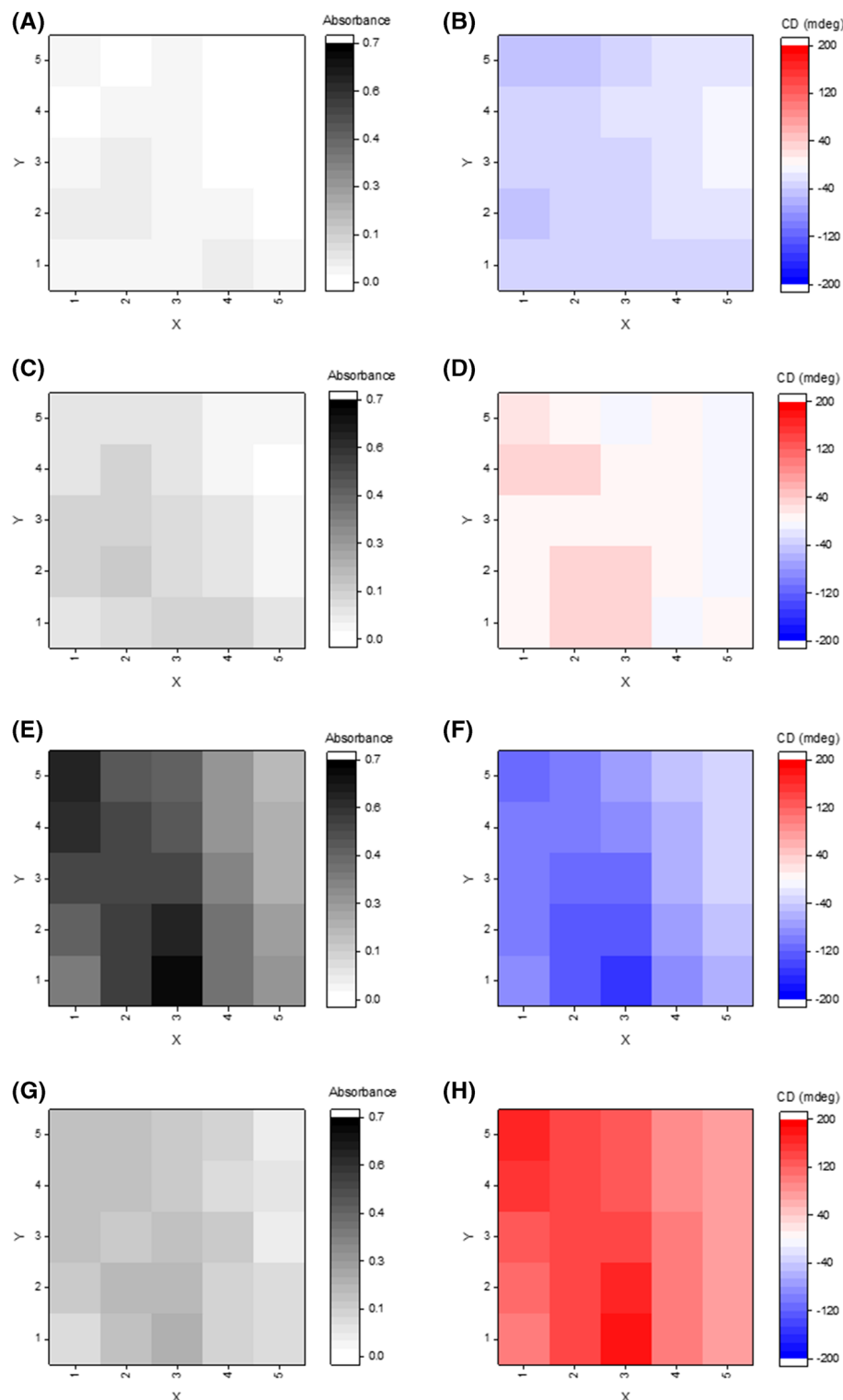


FIGURE 11 2D optical activity maps of a cast film of **PhO(R,R) EP DPP NH** in THF. Absorbance versus X-Y (gray hues) and CD intensity versus X-Y (red and blue hues) for each of the wavelengths that had the most intense optical activity 294 nm (A and B), 326 nm (C and D), 546 nm (E and F), and 582 nm (G and H); each square represents a $50 \times 50 \mu\text{m}$ area where the center was illuminated.

The inconsistencies in intensity between absorbance and optical activity are most evident at 294 nm (maps A and B), where the strongest absorbance is observed in squares (1,2), (2,2), (2,3), and (4,1), whereas the most intense optical activity is observed in squares (1,2), (1,5), and (2,5), suggesting contributions from linear dichroism and/or birefringence. For 326 nm (Map D), both positive and negative signals are observed. Rotation of the sample by 180° displays a change in intensity of the Cotton effect at 562 nm, further evidence of the aforementioned additional factors (Supporting information S1: ESI 5.64). These are likely a product of the deposition method, given the previously observed sensitivity of thin film formation technique on the supramolecular ordering and homogeneity.¹³⁰

2.8 | Monolayer formation

Scanning tunneling microscopy (STM) has been utilized to study the self-assembly of DPP derivatives.^{76,131} Hence, STM studies were undertaken to see how the **PhO(S,S) EP DPP NH** molecules organized on a highly oriented pyrolytic graphite (HOPG) surface. The monolayer was grown from immersion of HOPG in a 10^{-5} mol dm⁻³ THF solution and imaging in a drop of phenyl octane. **PhO(S,S) EP DPP NH** formed well-defined lamellae of the nature seen in Figure 12 and Supporting information S1: ESI 5.65, displaying good uniformity, with defects in packing being rare (Supporting information S1: ESI 5.66). Lamellar dimensions were equivalent to that of a single molecule of **PhO(S,S) EP DPP NH** and stacked in a slipped stacked manner (Figure 12 and Supporting information S1: ESI 5.67), likely driven by the hydrogen

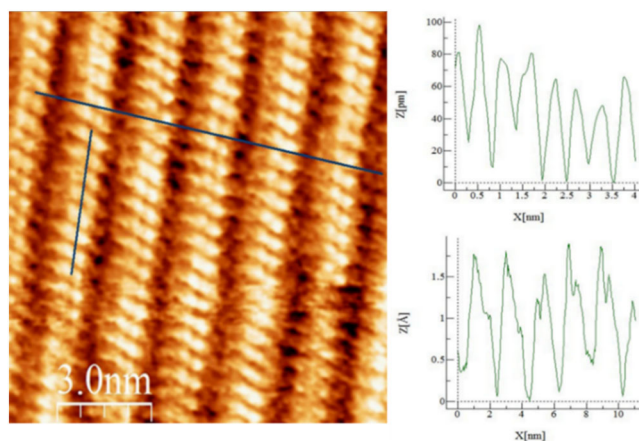


FIGURE 12 Self-assembled monolayer of **PhO(S,S) EP DPP NH** formed from 10^{-5} mol dm⁻³ THF solution on HOPG imaging in a phenyl octane droplet ($V_{\text{bias}} = -700$ mV $I_{\text{set}} = 300$ pA). Inset profiles showing lamella width and length.

bonding and close packing.⁷⁶ The dynamic nature of the self-assembled structure is evidenced by the formation and disappearance of a hole upon continual scanning (Supporting information S1: ESI 5.68). The tilt of the cores with respect to the lamellar axis is unique for each enantiomer and shows how the established transfer of chirality from stereogenic centers to monolayer structure¹³² can also be applied in these molecules.

3 | CONCLUSION

We have synthesized the novel pair of π -functional enantiomeric chiral chromophores in good yield (53%–56%). The compounds display excellent photophysical properties for light-harvesting ($\epsilon = 54,100$ dm³mol⁻¹ cm⁻¹) and emissive ($\Phi = 0.89$) applications in solution. Electronically, the materials behave as donor-type systems with a two-electron irreversible oxidation and single electron quasi-reversible reduction, with hydrogen bonding inhibiting the stabilization of the radical cation species formed in the redox process. Thin film absorption spectra, from drop-cast THF solutions, show a broadening and bathochromic shift compared with solution spectra, owing to the intermolecular hydrogen bonding and π - π stacking in the solid state. Optical band gaps of 2.0 eV give good agreement with cyclic voltammetry measurements. STM measurements show that for monolayers formed from immersion of HOPG in THF solutions, molecules arrange into 1D lamellae. Monomeric CD spectra are observed in THF, with no perceived aggregation, whereas in the solid-state enhancement of CD is observed with a positive excitonic couplet at 562 nm. In solvents that promote aggregation, CD spectra display Cotton effects at ≈ 567 and at ≈ 355 nm, both of the same sign, depending on the enantiomer. In ethanol, the molecules aggregate giving a significant increase in $\Delta\epsilon$ when compared with acetone ($\Delta\epsilon \approx \pm 15$ vs. $\Delta\epsilon \approx \pm 3.4$). Heating to dissolution leads to loss of the *J*-aggregate band in absorption and diminished CD signal, which fails to return at a cooling rate of 2.5°C/min, suggesting that the structures are former under kinetic rather than thermodynamic control. Owing to the emissive nature of the compounds, CPL is also observed. In said solvent systems that promote aggregation at concentrations of 0.1–0.2 mg/ml, after heating to solubilization and cooling at 1°C/min, helical fibers are observed, with the twist seemingly dictated by the molecular chirality at the stereogenic center. Self-assembly of the helical fibers is likely driven by the interplay between intermolecular hydrogen bonding and π - π stacking,¹³³ with hydrogen-bonding driving assembly of these structures and chirality dictating the twisting direction.¹³⁴ Literature precedent shows that often similar

systems tend to form hydrogen-bonded oligomers, which assemble into disordered stacks that ultimately lead to the formation of a chiral helix.^{133,135–140} From the evidence displayed, it seems that in THF the system, it self-assembles to form lamellar structures. In solvent systems that promote aggregation, helical structures are formed, as well as through vapor diffusion into THF solutions. In such solvents that promote the formation of helical aggregates, when a racemic mixture is utilized, straight plate-type structures are produced, with no twisting. When helical structures are deposited on a surface of quartz or mica, unraveling of the fiber at the surface can occur, forming plate-type structures, similar to observations for the racemic mixture and akin to the lamellae from STM. This suggests the fact that oligomers are formed as straight plate lamellar assemblies and then a defect promotes the twist, be it through solvent interaction¹³³ or another means, and the helicity is dictated by molecular chirality. From an optoelectronic device point of view, solvent dictation of morphology is particularly interesting especially in the case of potential vapor annealing to change morphology from a lamellae structure to a helical system and the subsequent influence on performance. Future design of materials could look to increase conjugation while retaining the favorable optoelectronic and self-assembly properties of the subjects of this article or their use as a morphological additive through a sergeants and soldiers' chiral induction approach¹⁴¹ to dictate morphology of state-of-the-art donors. Ultimately, this may lead to organic semiconductors with long charge carrier lifetimes.¹⁴² The DPPs are particularly promising in this regard.¹⁴³ In a broader sense, they could also lead to new properties arising from the molecular chirality and charge transfer properties,^{144,145} including those displayed by twisted crystals.^{146,147}

ACKNOWLEDGMENTS

We thank Engineering and Physical Sciences Research Council (project EP/M005178/1) and the University of Nottingham for funding (including BNSCF421 and the Propulsion Futures Beacon of Excellence). We thank Dr. Mick Cooper and Mr. Ben Pointer-Gleadhill for mass spectrometry assistance; Mr. Shazad Aslam, Mr. Kevin Butler, and Dr. Adrienne Davis for NMR assistance; Nicola Weston and the NMRC for SEM studies; and Mr. Tom Clayton and Mr. Mark Guyler for laboratory assistance. We warmly thank Dr. Tamás Jávorfí at B23, Diamond Light Source, Ltd. for assistance in collecting spatially resolved CD spectra.

DATA AVAILABILITY STATEMENT

The data that support the findings of this study are available in the Supporting information S1 of this article,


which can be found in the online version of this article at the publisher's website.

ORCID

Joshua Humphreys  <https://orcid.org/0000-0002-4867-2936>

C. Elizabeth Killalea  <https://orcid.org/0000-0002-6095-2586>

Flavia Pop  <https://orcid.org/0000-0003-3524-9781>

Giuliano Siligardi  <https://orcid.org/0000-0002-4667-6423>

David B. Amabilino  <https://orcid.org/0000-0003-1674-8462>

REFERENCES

- Schenning APHJ, Meijer EW. Supramolecular electronics; nanowires from self-assembled pi-conjugated systems. *Chem Commun.* 2005;26:3245–3258.
- Schenning APHJ, Jonkheijm P, Hoeben FJM, et al. Towards supramolecular electronics. *Synth Met.* 2004;147(1-3):43–48.
- Chen H, Stoddart JF. From molecular to supramolecular electronics. *Nat Rev Mater.* 2021;6(9):804–828.
- Shi X, Bao WW. Hydrogen-bonded conjugated materials and their application in organic field-effect transistors. *Front Chem.* 2021;9:1–6.
- Ávila-Rovelo NR, Ruiz-Carretero A. Recent progress in hydrogen-bonded π -conjugated systems displaying J-type aggregates. *Org Mater.* 2020;2(01):047–063.
- García AM, Martínez G, Ruiz-Carretero A. The importance of spin state in chiral supramolecular electronics. *Front Chem.* 2021;9:1–9.
- Moulin E, Busseron E, Giuseppone N. *Supramolecular materials for opto-electronics*. The Royal Society of Chemistry; 2015:1–52.
- Dumele O, Chen J, Passarelli JV, Stupp SI. Supramolecular energy materials. *Adv Mater.* 2020;32(17):1–32.
- Scharber MC, Sariciftci NS. Efficiency of bulk-heterojunction organic solar cells. *Prog Polym Sci.* 2013;38(12):1929–1940.
- Watkins PK, Walker AB, Verschoor GLB. Dynamical Monte Carlo modelling of organic solar cells: the dependence of internal quantum efficiency on morphology. *Nano Lett.* 2005; 5(9):1814–1818.
- Liu Y, Zhang C, Hao D, et al. Enhancing the performance of organic solar cells by hierarchically supramolecular self-assembly of fused-ring electron acceptors. *Chem Mater.* 2018; 30(13):4307–4312.
- Głowacki ED, Irimia-Vladu M, Bauer S, Sariciftci NS. Hydrogen-bonds in molecular solids—from biological systems to organic electronics. *J Mater Chem B.* 2013;1(31):3742–3753.
- Kumar M, Kumar S. Liquid crystals in photovoltaics: a new generation of organic photovoltaics. *Polym J.* 2017;49(1): 85–111.
- Babu SS, Prasanthkumar S, Ajayaghosh A. Self-assembled gelators for organic electronics. *Angew Chem Int Ed.* 2012; 51(8):1766–1776.
- Chu CC, Raffy G, Ray D, et al. Self-assembly of supramolecular fullerene ribbons via hydrogen-bonding interactions and

- their impact on fullerene electronic interactions and charge carrier mobility. *J Am Chem Soc.* 2010;132(36):12717-12723.
16. Sytnyk M, Głowacki ED, Yakunin S, et al. Hydrogen-bonded organic semiconductor micro- and nanocrystals: from colloidal syntheses to (opto-)electronic devices. *J Am Chem Soc.* 2014;136(47):16522-16532.
 17. Haruk AM, Mativetsky JM. Supramolecular approaches to nanoscale morphological control in organic solar cells. *Int J Mol Sci.* 2015;16(6):13381-13406.
 18. Liu T, Huo L, Chandrabose S, et al. Optimized fibril network morphology by precise side-chain engineering to achieve high-performance bulk-heterojunction organic solar cells. *Adv Mater.* 2018;30(26):1-8.
 19. Weng K, Ye L, Zhu L, et al. Optimized active layer morphology toward efficient and polymer batch insensitive organic solar cells. *Nat Commun.* 2020;11(1):1-9.
 20. Grzybowski M, Gryko DT. Diketopyrrolopyrroles: synthesis, reactivity, and optical properties. *Adv Opt Mater.* 2015;3(3):280-320.
 21. Kaur M, Choi DH. Diketopyrrolopyrrole: brilliant red pigment dye-based fluorescent probes and their applications. *Chem Soc Rev.* 2015;44(1):58-77.
 22. Sassi M, Buccheri N, Rooney M, et al. Near-infrared roll-off-free electroluminescence from highly stable diketopyrrolopyrrole light emitting diodes. *Sci Rep.* 2016;6(1):34096.
 23. Data P, Kurowska A, Pluczyk S, et al. Exciplex enhancement as a tool to increase OLED device efficiency. *J Phys Chem C.* 2016;120(4):2070-2078.
 24. Rasool S, Hoang QV, Van Vu D, et al. High-efficiency single and tandem fullerene solar cells with asymmetric monofluorinated diketopyrrolopyrrole-based polymer. *J Energy Chem.* 2021;64:236-245.
 25. Luo H, Yu C, Liu Z, et al. Remarkable enhancement of charge carrier mobility of conjugated polymer field-effect transistors upon incorporating an ionic additive. *Sci Adv.* 2016;2(5):1-11.
 26. Kang I, Yun HJ, Chung DS, Kwon SK, Kim YH. Record high hole mobility in polymer semiconductors via side-chain engineering. *J Am Chem Soc.* 2013;135(40):14896-14899.
 27. Naik MA, Venkatramiah N, Kanimozhi C, Patil S. Influence of side-chain on structural order and photophysical properties in thiophene based diketopyrrolopyrroles: a systematic study. *J Phys Chem C.* 2012;116(50):26128-26137.
 28. Wienk MM, Turbiez M, Gilot J, Janssen RAJ. Narrow-bandgap diketo-pyrrolo-pyrrole polymer solar cells: the effect of processing on the performance. *Adv Mater.* 2008;20(13):2556-2560.
 29. Kaur M, Cho MJ, Choi DH. Chemodosimeter approach: selective detection of fluoride ion using a diketopyrrolopyrrole derivative. *Dye Pigment.* 2014;103:154-160.
 30. Más-Montoya M, Janssen RAJ. The effect of H- and J-aggregation on the photophysical and photovoltaic properties of small thiophene-pyridine-DPP molecules for bulk-heterojunction solar cells. *Adv Funct Mater.* 2017;27(16):1605779.
 31. Tamayo AB, Tantiwivat M, Walker B, Nguyen TQ. Design, synthesis, and self-assembly of oligothiophene derivatives with a diketopyrrolopyrrole core. *J Phys Chem C.* 2008;112(39):15543-15552.
 32. Kim Y, Song CE, Cho A, et al. Synthesis of diketopyrrolopyrrole (DPP)-based small molecule donors containing thiophene or furan for photovoltaic applications. *Mater Chem Phys.* 2014;143(2):825-829.
 33. Schutting S, Borisov SM, Klimant I. Diketo-pyrrolo-pyrrole dyes as new colorimetric and fluorescent pH indicators for optical carbon dioxide sensors. *Anal Chem.* 2013;85(6):3271-3279.
 34. Glowacki ED, Coskun H, Blood-Forsythe MA, et al. Hydrogen-bonded diketopyrrolopyrrole (DPP) pigments as organic semiconductors. *Org Electron.* 2014;15(12):3521-3528.
 35. Yang J, Tan H, Li D, et al. Synthesis, two-photon absorption and aggregation-induced emission properties of multi-branched triphenylamine derivatives based on diketopyrrolopyrrole for bioimaging. *RSC Adv.* 2016;6(63):58434-58442.
 36. Ftouni H, Bolze F, Nicoud JF. Water-soluble diketopyrrolopyrrole derivatives for two-photon excited fluorescence microscopy. *Dye Pigment.* 2013;97(1):77-83.
 37. Yang C, Zheng M, Li Y, et al. N-monoalkylated 1,4-diketo-3,6-diphenylpyrrolo[3,4-c]pyrroles as effective one- and two-photon fluorescence chemosensors for fluoride anions. *J Mater Chem A.* 2013;1(16):5172-5178.
 38. Ruiz-Carretero A, Ávila Rovelo NR, Militzer S, Mésini PJ. Hydrogen-bonded diketopyrrolopyrrole derivatives for energy-related applications. *J Mater Chem A.* 2019;7(41):23451-23475.
 39. Stolte M, Suraru S-L, Diemer P, et al. Diketopyrrolopyrrole organic thin-film transistors: impact of alkyl substituents and tolerance of ethylhexyl stereoisomers. *Adv Funct Mater.* 2016;26(41):7415-7422.
 40. Liu LX, Yang Y, Wang YH, et al. Building supramolecular chirality in bulk heterojunctions enables amplified dissymmetry current for high-performing circularly polarized light detection. *ACS Mater Lett.* 2022;4(2):401-409.
 41. Albano G, Zinna F, Urraci F, et al. Aggregation modes of chiral diketopyrrolo[3,4-c]pyrrole dyes in solution and thin films. *Chem a Eur J.* 2022;28(51):e202201178.
 42. Suna Y, Nishida JI, Fujisaki Y, Yamashita Y. Ambipolar behavior of hydrogen-bonded diketopyrrolopyrrole-thiophene co-oligomers formed from their soluble precursors. *Org Lett.* 2012;14(13):3356-3359.
 43. Liu C, Dong S, Cai P, et al. Donor-acceptor copolymers based on thermally cleavable indigo, isoindigo, and DPP units: synthesis, field effect transistors, and polymer solar cells. *ACS Appl Mater Interfaces.* 2015;7(17):9038-9051.
 44. Yang K, Li X, Huang YF, et al. Investigation of hydrogen-bonding mediated molecular packing of diketopyrrolopyrrole based donor-acceptor oligomers in the solid state. *Polymer.* 2019;160:238-245.
 45. Sun B, Hong W, Aziz H, Li Y. Effective interfacial layer to enhance efficiency of polymer solar cells via solution-processed fullerene-surfactants. *J Mater Chem.* 2012;22(17):18950-18955.
 46. Mula S, Han T, Heiser T, et al. Hydrogen bonding as a supramolecular tool for robust OFET devices. *Chem - Eur J.* 2019;25(35):8304-8312.
 47. Pop F, Lewis W, Amabilino DB. Solid state supramolecular structure of diketopyrrolopyrrole chromophores: correlating stacking geometry with visible light absorption. *CrystEng-Comm.* 2016;18(46):8933-8943.

48. Dhar J, Karothu DP, Patil S. Herringbone to cofacial solid state packing via H-bonding in diketopyrrolopyrrole (DPP) based molecular crystals: influence on charge transport. *Chem Commun.* 2015;51(1):97-100.
49. Ocheje MU, Selivanova M, Zhang S, et al. Influence of amide-containing side chains on the mechanical properties of diketopyrrolopyrrole-based polymers. *Polym Chem.* 2018; 9(46):5531-5542.
50. Ma J, Liu Z, Yao J, et al. Improving ambipolar semiconducting properties of thiazole-flanked diketopyrrolopyrrole-based terpolymers by incorporating urea groups in the side-chains. *Macromolecules.* 2018;51(15):6003-6010.
51. Zheng Y, Ashizawa M, Zhang S, et al. Tuning the mechanical properties of a polymer semiconductor by modulating hydrogen bonding interactions. *Chem Mater.* 2020;32(13): 5700-5714.
52. Yao J, Yu C, Liu Z, et al. Significant improvement of semiconducting performance of the diketopyrrolopyrrole-quaterthiophene conjugated polymer through side-chain engineering via hydrogen-bonding. *J Am Chem Soc.* 2016;138(1): 173-185.
53. Ogi S, Fukaya N, Arifin SBB, Hijikata Y, Yamaguchi S. Seeded polymerization of an amide-functionalized diketopyrrolopyrrole dye in aqueous media. *Chem - Eur J.* 2019;25(30):7303-7307.
54. Du W, Ohayon D, Combe C, et al. Improving the compatibility of diketopyrrolopyrrole semiconducting polymers for biological interfacing by lysine attachment. *Chem Mater.* 2018; 30(17):6164-6172.
55. Aytun T, Barreda L, Ruiz-Carretero A, Lehrman JA, Stupp SI. Improving solar cell efficiency through hydrogen bonding: a method for tuning active layer morphology. *Chem Mater.* 2015;27(4):1201-1209.
56. Ghosh S, Das S, Saeki A, Praveen VK, Seki S, Ajayaghosh A. A hybrid organogel of a low band gap diketopyrrolopyrrole with PC₇₁BM: phase separated morphology and enhanced photoconductivity. *ChemNanoMat.* 2018;4(8):831-836.
57. Militzer S, Tran TMP, Mésini PJ, Ruiz-Carretero A. Tuning the optical and self-assembly properties of diketopyrrolopyrrole semicarbazone derivatives through hydrogen bonding. *ChemNanoMat.* 2018;4(8):790-795.
58. Ghosh S, Raveendran R, Saeki A, Seki S, Namboothiry M, Ajayaghosh A. Charge carrier polarity modulation in diketopyrrolopyrrole-based low band gap semiconductors by terminal functionalization. *ACS Appl Mater Interfaces.* 2019; 11(1):1088-1095.
59. Militzer S, Nishimura N, Ávila-Rovelo NR, et al. Impact of chirality on hydrogen-bonded supramolecular assemblies and photoconductivity of diketopyrrolopyrrole derivatives. *Chem - Eur J.* 2020;26(44):9998-10004.
60. Maity S, Bedi A, Patil S. Side-chain induced chirality in diketopyrrolopyrrole based polymers. *J Polym Sci A.* 2021; 59(24):3181-3188.
61. Talamo MM, Pop F, Avarvari N. Straightforward N-alkylation of diketopyrrolopyrroles through the Mitsunobu reaction with benzyl, alpha-branched, and chiral alcohols. *Chem Commun.* 2021;57(53):6514-6517.
62. Biswas S, Kumar M, Levine AM, Jimenez I, Ulijn RV, Braunschweig AB. Visible-light photooxidation in water by O-1(2)-generating supramolecular hydrogels. *Chem Sci.* 2020; 11(16):4239-4245.
63. Rieth S, Li Z, Hinkle CE, et al. Superstructures of diketopyrrolopyrrole donors and perylene diimide acceptors formed by hydrogen-bonding and $\pi\cdots\pi$ stacking. *J Phys Chem C.* 2013; 117(21):11347-11356.
64. Zerdan RB, Shewmon NT, Zhu Y, et al. The influence of solubilizing chain stereochemistry on small molecule photovoltaics. *Adv Funct Mater.* 2014;24(38):5993-6004.
65. Hume PA, Monks JP, Pop F, Davies ES, MacKenzie RCI, Amabilino DB. Self-assembly of chiral-at-end diketopyrrolopyrroles: symmetry dependent solution and film optical activity and photovoltaic performance. *Chem - Eur J.* 2018;24(54): 14461-14469.
66. Gao T, Jiang Z, Chen B, et al. Axial chiral binaphthalene-diketopyrrolopyrrole dyads as efficient far-red to near-infrared circularly polarized luminescent emitters. *Dye Pigment.* 2020; 173:107998.
67. Dhbaibi K, Favereau L, Srebro-Hooper M, et al. Exciton coupling in diketopyrrolopyrrole-helicene derivatives leads to red and near-infrared circularly polarized luminescence. *Chem Sci.* 2018;9(3):735-742.
68. Dhbaibi K, Shen C, Jean M, et al. Chiral diketopyrrolopyrrole-helicene polymer with efficient red circularly polarized luminescence. *Front Chem.* 2020;8:2-9.
69. Draper ER, Dietrich B, Adams DJ. Self-assembly, self-sorting, and electronic properties of a diketopyrrolopyrrole hydrogelator. *Chem Commun.* 2017;53(11):1864-1867.
70. Thool GS, Narayanaswamy K, Venkateswararao A, et al. Highly directional 1D supramolecular assembly of new diketopyrrolopyrrole-based gel for organic solar cell applications. *Langmuir.* 2016;32(17):4346-4351.
71. Ruiz-Carretero A, Aytun T, Bruns CJ, Newcomb CJ, Tsai WW, Stupp SI. Stepwise self-assembly to improve solar cell morphology. *J Mater Chem A.* 2013;1(38):11674-11681.
72. Soberats B, Hecht M, Würthner F. Diketopyrrolopyrrole columnar liquid-crystalline assembly directed by quadruple hydrogen bonds. *Angew Chem Int Ed.* 2017;56(36):10771-10774.
73. Wang K, Bohra H, Gonçalves RA, et al. Multiscale self-assembly of a phenyl-flanked diketopyrrolopyrrole derivative: a solution-processable building block for π -conjugated supramolecular polymers. *Langmuir.* 2019;35(16):5626-5634.
74. Humphreys J, Pop F, Hume PA, et al. Solid state structure and properties of phenyl diketopyrrolopyrrole derivatives. *CrystEngComm.* 2021;23(8):1796-1814.
75. Calvo-Castro J, McHugh CJ. Exploring structure based charge transport relationships in phenyl diketopyrrolopyrrole single crystals using a 2D π - π dimer model system. *J Mater Chem C.* 2017;5(16):3993-3998.
76. Fu C, Beldon PJ, Perepichka DF. H-bonding control of supramolecular ordering of diketopyrrolopyrroles. *Chem Mater.* 2017;29(7):2979-2987.
77. Honda A, Tamaki Y, Miyamura K. The effects of noncovalent interactions on surface structures formed by diketopyrrolopyrrole pigment and its alkyl-derivatives on HOPG substrate. *Bull Chem Soc Jpn.* 2015;88(7):969-975.
78. Ciba Specialty Chemicals Corporation, USPat, 5969154, 1999.

79. Mitsunobu O. The use of diethylazodicarboxylate and triphenylphosphine in synthesis and transformation of natural products. *Synthesis*. 1981;1(01):1-28.
80. Swamy KCK, Kumar NNB, Balaraman E, Kumar KVPP. Mitsunobu and related reactions: advances and applications. *Chem Rev*. 2009;109(6):2551-2651.
81. Amabilino DB, Ramos E, Serrano J-L, Sierra T, Veciana J. Long-range chiral induction in chemical systems with helical organization—promesogenic monomers in the formation of poly (isocyanides) and in the organization of liquid crystals. *J Am Chem Soc*. 1998;120(36):9126-9134.
82. Iavicoli P, Xu H, Keszthelyi T, et al. Organization of the enantiomeric and racemic forms of an amphiphilic resorcinol derivative at the air–water and graphite–1-phenyloctane interfaces. *Chirality*. 2012;24(2):155-166.
83. Saletta WJ. *Transfer of chirality from amphiphiles into materials*, PhD Thesis., Universitat Autònoma de Barcelona; 2013. <http://hdl.handle.net/10803/125861>
84. Sangwal K. Effects of impurities on crystal growth processes. *Prog Cryst Growth Charact*. 1996;32(1-3):3-43.
85. Schnitzer T, Preuss MD, van Basten J, et al. How subtle changes can make a difference: reproducibility in complex supramolecular systems. *Angew Chem Int Ed*. 2022;61(41):e202206738.
86. Beaujuge PM, Amb CM, Reynolds JR. Spectral engineering in π -conjugated polymers with intramolecular donor–acceptor interactions. *Acc Chem Res*. 2010;43(11):1396-1407.
87. Luňák S, Vala M, Vyňuchal J, et al. Absorption and fluorescence of soluble polar diketo-pyrrolo-pyrroles. *Dye Pigment*. 2011;91(3):269-278.
88. Vala M, Vyňuchal J, Toman P, Weiter M, Luňák S. Novel, soluble diphenyl-diketo-pyrrolo-pyrroles: experimental and theoretical study. *Dye Pigment*. 2010;84(2):176-182.
89. Vala M, Krajčovič J, Luňák S, Ouzzane I, Bouillon JP, Weiter M. HOMO and LUMO energy levels of N,N'-dinitrophenyl-substituted polar diketopyrrolopyrroles (DPPs). *Dye Pigment*. 2014;106:136-142.
90. Vala M, Weiter M, Vyňuchal J, Toman P, Luňák S. Comparative studies of diphenyl-diketo-pyrrolo-pyrrole derivatives for electroluminescence applications. *J Fluoresc*. 2008;18(6):1181-1186.
91. Luňák S, Vyňuchal J, Vala M, Havel L, Hrdina R. The synthesis, absorption and fluorescence of polar diketo-pyrrolo-pyrroles. *Dye Pigment*. 2009;82(2):102-108.
92. Aigner D, Ungerböck B, Mayr T, Saf R, Klimant I, Borisov SM. Fluorescent materials for pH sensing and imaging based on novel 1,4-diketopyrrolo-[3,4-c]pyrrole dyes. *J Mater Chem C*. 2013;1(36):5685-5693.
93. Yoon WS, Kim DW, Park JM, et al. A novel bis-lactam acceptor with outstanding molar extinction coefficient and structural planarity for donor–acceptor type conjugated polymer. *Macromolecules*. 2016;49(22):8489-8497.
94. Sambathkumar B, Kumar PSV, Deepakrao FS, et al. Two donor–one acceptor random terpolymer comprised of diketopyrrolopyrrole quaterthiophene with various donor π -linkers for organic photovoltaic application. *J Phys Chem C*. 2016;120(47):26609-26619.
95. Erbas SC, Alp S. Synthesis and spectroscopic studies of N,N'-dialkyl derivatives of antisymmetrical 2H,5H-sihdropyrrolo [3,4-c]pyrrole-1,4-diones. *J Fluoresc*. 2014;24(2):329-335.
96. Grzybowski M, Glodkowska-Mrowka E, Clermont G, Blanchard-Desce M, Gryko DT. Synthesis and optical properties of water-soluble diketopyrrolopyrroles. *Chem Heterocycl Compd*. 2017;53(1):72-77.
97. Purc A, Banasiewicz M, Glodkowska-Mrowka E, Gryko DT. Modulation of the fluorescence properties of diketopyrrolopyrroles via various electron-rich substituents. *J Mater Chem C*. 2016;4(14):2877-2885.
98. Wallquist O, Lenz R. 20 years of DPP pigments—future perspectives. *Macromol Symp*. 2002;187(1):617-630.
99. Wang C, Qin Y, Sun Y, Guan YS, Xu W, Zhu D. Thiophene-diketopyrrolopyrrole-based quinoidal small molecules as solution-processable and air-stable organic semiconductors: tuning of the length and branching position of the alkyl side chain toward a high-performance n-channel organic field-effect transistor. *ACS Appl Mater Interfaces*. 2015;7(29):15978-15987.
100. Qiao Y, Guo Y, Yu C, et al. Diketopyrrolopyrrole-containing quinoidal small molecules for high-performance, air-stable, and solution-processable n-channel organic field-effect transistors. *J Am Chem Soc*. 2012;134(9):4084-4087.
101. Gora M, Pluczyk S, Zassowski P, et al. EPR and UV–vis spectroelectrochemical studies of diketopyrrolopyrroles disubstituted with alkylated thiophenes. *Synth Met*. 2016;216:75-82.
102. Wiosna-Salyga G, Gora M, Zagorska M, et al. Diketopyrrolopyrroles disubstituted with alkylated thiophenes: effect of the donor unit size and solubilizing substituents on their redox, photo- and electroluminescence properties. *RSC Adv*. 2015;5(73):59616-59629.
103. Danila I, Riobé F, Piron F, et al. Hierarchical chiral expression from the nano- to mesoscale in synthetic supramolecular helical fibers of a nonamphiphilic C₃-symmetrical π -functional molecule. *J Am Chem Soc*. 2011;133(21):8344-8353.
104. Danila I, Pop F, Escudero C, et al. Twists and turns in the hierarchical self-assembly pathways of a non-amphiphilic chiral supramolecular material. *Chem Commun*. 2012;48(38):4552-4554.
105. Neo WT, Ye Q, Shi Z, Chua S, Xu J. Control of morphology and performance of diketopyrrolopyrrole-based electrochromic polymers using solvent vapor annealing. *J Polym Res*. 2018;25(3):68.
106. Wang JL, Wu Z, Miao JS, et al. Solution-processed diketopyrrolopyrrole-containing small-molecule organic solar cells with 7.0% efficiency: in-depth investigation on the effects of structure modification and solvent vapor annealing. *Chem Mater*. 2015;27(12):4338-4348.
107. Bernauer F. *'Gedrillite' Kristalle: Verbreitung Entstehungsweise und Beziehungen zu optischer Aktivität und Molekularsymmetrie*. Berlin: Gerbrüder Borntraeger; 1929.
108. Shtukenberg AG, Punin YO, Gujral A, Kahr B. Growth actuated bending and twisting of single crystals. *Angew Chem Int Ed*. 2014;53(3):672-699.
109. Killalea CE, Amabilino DB. Stereochemistry and twisted crystals. *Isr J Chem*. 2021;61(9-10):629-644.
110. Giraldo O, Brock SL, Marquez M, Suib SL, Hillhouse H, Tsapatsis M. Spontaneous formation of inorganic helices. *Nature*. 2000;405(6782):38.

111. Li CY, Yan D, SZD C, et al. Double-twisted helical lamellar crystals on a synthetic main-chain chiral polyester similar to biological polymers. *Macromolecules*. 1999;32(2):524-527.
112. Shtukenberg AG, Gujral A, Rosseeva E, Cui X, Kahr B. Mechanics of twisted hippuric acid crystals untwisting as they grow. *CrystEngComm*. 2015;17:8817-8824.
113. Ho DM, Pascal RA. Decacyclene: a molecular propeller with helical crystals. *Chem Mater*. 1993;5(9):1358-1361.
114. Maillard D, Prud'homme RE. Crystallization of ultrathin films of polylactides: from chain chirality to lamella curvature and twisting. *Macromolecules*. 2008;48(5):1705-1712.
115. Amabilino DB, Dizon GC, Killalea CE, Malia AR. *Fundamentals of supramolecular Chirality*. London: World Scientific Publishing Europe Ltd; 2022:1-58.
116. Bierman MJ, Lau YK, Kvit AV, Schmitt AL, Kin S. Dislocation-driven nanowire growth and Eshelby twist. *Science*. 2008;320(5879):1060-1063.
117. Kuwabara J, Kawasaki R, Yasuda T, Kanbara T. Hydrogen-bonded dimers of mono-alkylated diketopyrrolopyrroles and their physical properties. *Synth Met*. 2022;284:117007.
118. Minguet M, Amabilino DB, Vidal-Gancedo J, Wurst K, Veciana J. Racemic and enantiomerically pure phenyl alpha-nitronyl nitroxide radicals: influence of chirality on solution and solid state properties. *J Mater Chem*. 2002;12(3):570-578.
119. Qian WJ, Gonzalez-Campo A, Perez-Rodriguez A, et al. Boosting self-assembly diversity in the solid-state by chiral/non-chiral Zn-II-porphyrin crystallization. *Chem - Eur J*. 2018;24(49):12950-12960.
120. Brewer A, Siligardi G, Neylon C, Stulz E. Introducing structural flexibility into porphyrin-DNA zipper arrays. *Org Biomol Chem*. 2011;9(3):777-782.
121. Tanaka H, Inoue Y, Mori T. Circularly polarized luminescence and circular dichroisms in small organic molecules: correlation between excitation and emission dissymmetry factors. *ChemPhotoChem*. 2018;2(5):386-402.
122. Schippers PH, van der Ploeg JPM, Dekkers HPJM. Circular polarization in the fluorescence of β γ -enones: distortion in the $^1n\pi^*$ state. *J Am Chem Soc*. 1983;105(1):84-89.
123. Ma K, Chen WJ, Jiao TF, et al. Boosting the circularly polarized luminescence of small organic molecules via multi-dimensional morphology control. *Chem Sci*. 2019;10(28):6821-6827.
124. Zhang YD, Yu S, Han B, et al. Circularly polarized luminescence in chiral materials. *Matter*. 2022;5(3):837-875.
125. Claborn K, Puklin-Faucher E, Kurimoto M, Kaminsky W, Kahr B. Circular dichroism imaging microscopy: application to enantiomorphous twinning in biaxial crystals of 1,8-dihydroxyanthraquinone. *J Am Chem Soc*. 2003;125(48):14825-14831.
126. Kaminsky W, Claborn K, Kahr B. Polarimetric imaging of crystals. *Chem Soc Rev*. 2004;33(8):514-525.
127. Hussain R, Javorfi T, Siligardi G. CD imaging at high spatial resolution at diamond B23 beamline: evolution and applications. *Front Chem*. 2021;9:616928.
128. Zinna F, Resta C, Górecki M, et al. Circular dichroism imaging: mapping the local supramolecular order in thin films of chiral functional polymers. *Macromolecules*. 2017;50(5):2054-2060.
129. Albano G, Górecki M, Pescitelli G, et al. Electronic circular dichroism imaging (CD i) maps local aggregation modes in thin films of chiral oligothiophenes. *New J Chem*. 2019;43(36):14584-14593.
130. Killalea CE, Samperi M, Siligardi G, Amabilino DB. Imaging deposition-dependent supramolecular chiral organisation. *Chem Commun*. 2022;58(28):4468-4471.
131. Jaroch T, Maranda-Niedbała A, Góra M, et al. Supramolecular organization of bi- and terthiophene disubstituted diketopyrrolopyrrole, donor-acceptor-donor semiconducting derivatives. *Synth Met*. 2015;204:133-140.
132. Elemans JAAW, De Cat I, Xu H, De Feyter S. Two-dimensional chirality at liquid-solid interfaces. *Chem Soc Rev*. 2009;38(3):722-736.
133. Yashima E, Ousaka N, Taura D, Shimomura K, Ikai T, Maeda K. Supramolecular helical systems: helical assemblies of small molecules, foldamers, and polymers with chiral amplification and their functions. *Chem Rev*. 2016;116(22):13752-13990.
134. Hidaka H, Murata M, Onai T. Helical aggregates of chiral N-(2-hydroxydodecyl) amino acids. *J Chem Soc Chem Commun*. 1984;9:562-564.
135. Hifsudheen M, Mishra RK, Vedhanarayanan B, Praveen VK, Ajayaghosh A. The helix to super-helix transition in the self-assembly of π -systems: superseding of molecular chirality at hierarchical level. *Angew Chem Int Ed*. 2017;56(41):12634-12638.
136. Korevaar PA, George SJ, Markvoort AJ, et al. Pathway complexity in supramolecular polymerization. *Nature*. 2012;481(7382):492-496.
137. Zhang L, Yang L, He Y, Han J-M. Helical perylene diimide self-assembly with a redox-active molecular switch applied to humidity sensing. *J Mater Chem A*. 2022;10(35):18363-18373.
138. Ghosh S, Li XQ, Stepanenko V, Würthner F. Control of H- and J-type π stacking by peripheral alkyl chains and self-sorting phenomena in perylene bisimide homo- and heteroaggregates. *Chem - Eur J*. 2008;14(36):11343-11357.
139. Hanabusa K, Yamada M, Kimura M, Shirai H. Prominent gelation and chiral aggregation of alkylamides derived from *trans*-1,2-diaminocyclohexane. *Angew Chem Int Ed*. 1996;35(17):1949-1951.
140. Smulders MMJ, Schenning APHJ, Meijer EW. Insight into the mechanisms of cooperative self-assembly: the "sergeants-and-soldiers" principle of chiral and achiral C_3 -symmetrical discotic triamides. *J Am Chem Soc*. 2008;130(12):606-611.
141. Prins LJ, Timmerman P, Reinhoudt DN. Amplification of chirality: the "sergeants and soldiers" principle applied to dynamic hydrogen-bonded assemblies. *J Am Chem Soc*. 2001;123(42):10153-10163.
142. Ávila-Rovelo NR, Martinez G, Matsuda W, et al. Hydrogen-bonded organic semiconductors with long charge carrier lifetimes. *J Phys Chem C*. 2022;126(26):10932-10939.
143. Ghosh S, Shankar S, Philips DS, Ajayaghosh A. Diketopyrrolopyrrole-based functional supramolecular polymers: next-

- generation materials for optoelectronic applications. *Mater Today Chem.* 2020;16:100242.
144. Wade J, Brandt JR, Reger D, et al. 500-fold amplification of small molecule circularly polarised luminescence through circularly polarised FRET. *Angew Chem Int Ed.* 2021;60(1):222-227.
 145. Ward MD, Shi WD, Gasparini N, Nelson J, Wade J, Fuchter MJ. Best practices in the measurement of circularly polarised photodetectors. *J Mater Chem C.* 2022;10(29):10452-10463.
 146. Yang YF, de Moraes LS, Ruzie C, et al. Charge transport in twisted organic semiconductor crystals of modulated pitch. *Adv Mater.* 2022;34(38):2203842.
 147. Yang YF, Zhang YZ, Hu CH, et al. Transport in twisted crystalline charge transfer complexes. *Chem Mater.* 2022;34(4):1778-1788.

SUPPORTING INFORMATION

Additional supporting information can be found online in the Supporting Information section at the end of this article.

How to cite this article: Humphreys J, Killalea CE, Pop F, Davies ES, Siligardi G, Amabilino DB. Self-assembly of chiral diketopyrrolopyrrole chromophores giving supramolecular chains in monolayers and twisted microtapes. *Chirality.* 2023;35(5):281-297. doi:10.1002/chir.23539